ADVANCED MATERIALS
www.advmat.de

Magnetospinning of Nano- and Microfibers

*Alexander Tokarev, Oleksandr Trotsenko, Ian M. Griffiths, Howard A. Stone, and Sergiy Minko**

A ferrofluid is a colloidal dispersion of stabilized magnetic nanoparticles that responds to an external magnetic field: above a critical value for a uniform field the surface of the ferrofluid deforms and a liquid spike is formed on the surface. In addition, as a magnet approaches an interface, the field is non-uniform, the interface deforms, and the liquid spike moves toward the magnet and forms a liquid bridge. This instability is explored in this work in a new method for drawing polymeric nano- and microfibers in which the magnetic force generated by a permanent magnet is used to draw fibers with controlled diameters in the 0.05–5 μm range. The magnetospinning technique demonstrated here is capable of producing highly loaded magnetic nano- and microfibers, porous nanofibers, composite nanofibers from various polymers and polymer composites, and materials with a low dielectric constant, e.g., Teflon.

Due to the very high surface-to-volume ratio and the microstructure that can be controlled at the molecular level, nanofibers find applications in composite materials, catalysis, filtration, and biomedicine.[1] A number of different methods have been developed to draw nanometer diameter fibers by stretching a liquid thread of polymer solutions or polymer melts by Coulomb forces or centrifugal forces that include electrospinning, force, and jet spinning.[2] The meltblown fiber extrusion technology has been successfully developed for polyolefin fibers from several micrometer down to tens of nanometers in diameter.[3] Alternatively, microfluidic spinning methods allow control over the fiber dimensions (from 50 nm to 100 μm) and allow reactive spinning when reactive liquids passing through microchannels can be rapidly mixed to react or inject into a precipitation bath.[4] The developed methods are broadly used because of the ability to vary the material properties and control the fiber diameter and its high production rates during the spinning of fibers from the free surface.[5] Many of the methods are well-scalable and have been commercialized. However, each of those methods has limitations related to processability of the polymers, their solubility, dielectric properties, miscibility, reactivity, etc.

Dr. A. Tokarev, O. Trotsenko, Prof. S. Minko
Nanostructured Materials Laboratory
University of Georgia
Athens, GA 30602, USA
E-mail: sminko@uga.edu
Dr. I. M. Griffiths
Mathematical Institute
University of Oxford
Oxford, OX2 6GG, UK
Prof. H. A. Stone
Department of Mechanical and Aerospace Engineering
Princeton University
Princeton, NJ 08544, USA

DOI: 10.1002/adma.201500374

A significant increase in interest associated with nanofibers calls for new methods that would be scalable, simple, readily implementable for fiber manufacturing in biological and biotechnological labs, and have productivity achievable for commercial/industrial scales of manufacturing similar to existing technologies such as meltblowing and electrospinning methods, but extend and secure additional possibilities for the fabrication of functional fibers. In this paper, we present a new method of fiber spinning, magnetospinning, which utilizes the stretching of ferrofluid droplets in a time-varying magnetic field to fabricate nanometer diameter fibers in a simple setup that is independent of the dielectric constant of the solvent and polymer used and can be scaled up and utilized for a wide range of materials and applications. Magnetically assisted electrospinning was previously described by Yang et al.[6] In this method, a magnetic field was used to align magnetic nanofibers after they were produced by electrospinning. The magnetospinning method described here is the first example where a magnetic field is used to draw polymer nanofibers.

A ferrofluid is a surfactant-stabilized colloidal dispersion of magnetic nanoparticles suspended in a host fluid.[7] Ferrofluids behave as ordinary liquids at zero magnetic field and exhibit properties of solids when the magnetic field is applied. Instabilities of ferrofluids in an external magnetic field have been studied intensively for several decades.[7,8] For example, when a magnetic field is applied perpendicular to a planar ferrofluid interface, conical shapes are observed on the surface. These spikes arise through energetically favorable balances between the magnetic force, gravity, and surface tension.[7] Once the field is removed the interfacial deformation vanishes.[9] Though seemingly understood scientifically, this phenomenon has found limited applications.[7,10] We demonstrate in this work that when a magnet is brought close to a ferrofluid surface, below a critical distance the interface deforms to form a liquid bridge connecting the bulk fluid to the magnet. Under certain operating regimes the liquid bridge is stable, which allows a fine fiber to be drawn by moving the magnet away from the surface, and continual evaporation of the solvent establishes the final properties of the fiber.

Magnetic nanoparticles with an average diameter of 9 ± 1.5 nm were synthesized by the co-precipitation method.[11] The particles were stabilized in chloroform by oleic acid and then mixed with polycaprolactone (PCL, see details in the Experimental Section). The concentration of magnetic nanoparticles was 5.75 wt%. The suspensions are dilute and have a Newtonian shear rheology (constant viscosity) as reported in the measurements in the Supporting Information. The resulting ferrofluid is used to draw fine fibers (see **Figure 1**a–d). Here, a spherical or rectangular (about 25 mm in size) magnet is glued onto a rotating circular stage (diameter 84 mm), whose angular velocity is controlled within ±5 revolutions per minute (RPM)

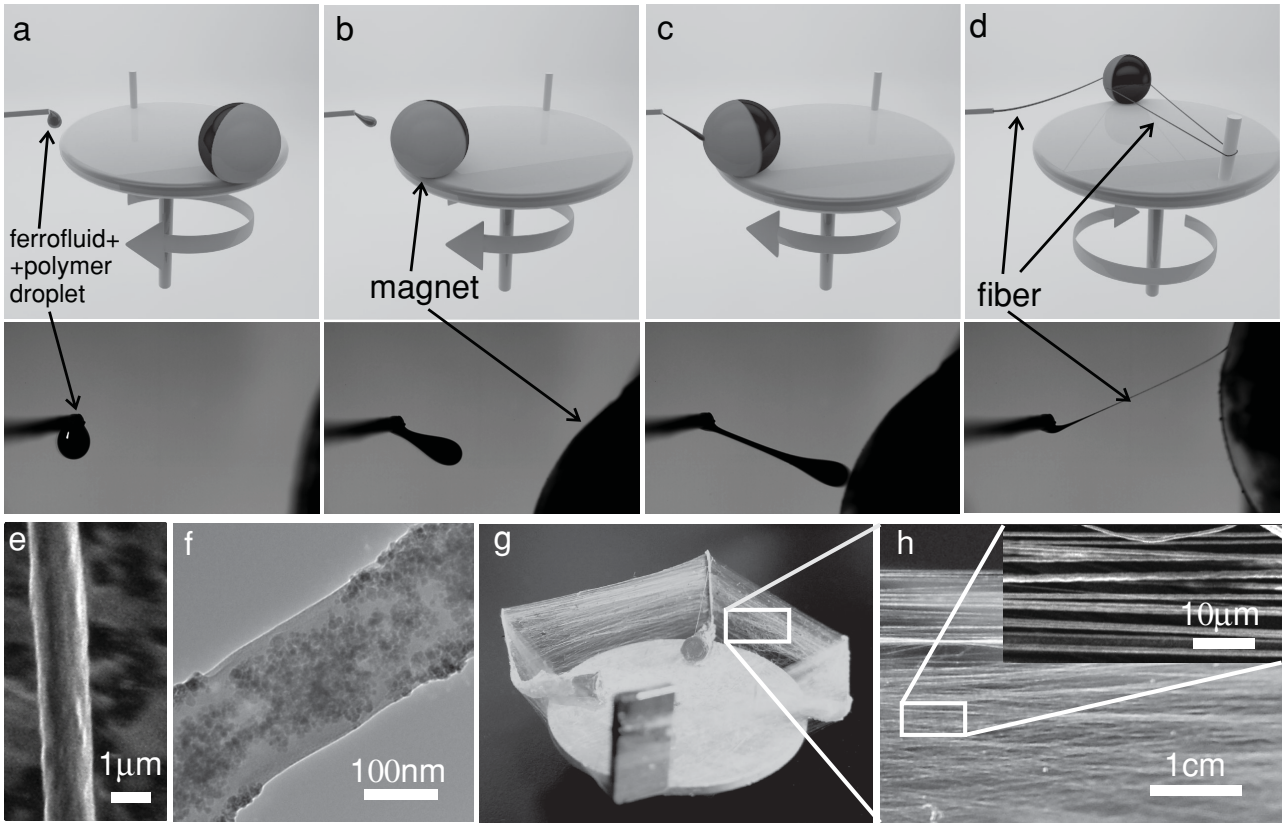

Figure 1. Schematic of the magnetospinning setup and the resulting PCL fibers. a) Polymer solution is pushed through the needle while a magnet is rotating on a circular stage. The gray and black colors represent, respectively, the north and south poles of the spherical magnet. b) As the magnet approaches the ferrofluid the magnetic force attracts the droplet toward the magnet and c) a liquid bridge between the magnet and the needle is formed. d) The magnet moves away and draws the polymer fiber while the solvent evaporates. The resulting nanofibers are spooled on a reel that is attached to the opposite side of the stage. e,f) SEM and TEM images of fabricated PCL fibers with a range of diameters. g,h) Photograph of ≈2500 nanofibers, produced in 5 min at 500 RPM. Inset in (h) shows SEM image of aligned nanofibers.

accuracy in the range of 50–1000 RPM. A syringe with a needle is connected to an automated pump and mounted on a 3D micromanipulator, which is used to maintain a precise distance of 6.5 mm between the tip of the needle and the magnet when the magnet passes the tip of the needle. As the magnet approaches the droplet (Figure 1a and Video S1, Supporting Information), the magnetic force attracts the droplet (Figure 1b). At a critical distance the droplet deforms and attaches to the magnet and a liquid bridge is formed (Figure 1c). As the stage continues to rotate, a continuous polymeric fiber is formed via drawing by the magnetic force while the solvent evaporates and the final properties of the fiber are established. The fibers are collected between the magnet and a reel glued on the opposite side of the stage (Figure 1d). A photograph of the magnetospinning setup that can be assembled within minutes can be found in the Supporting Information (Figure S1, Supporting Information). Figure 1g,h shows a bundle of approximately 2500 nanofibers, produced in 5 min at 500 RPM with a rectangular magnet and three bent needles for collecting fibers.

Three different magnetospinning regimes were discovered by varying the polymer concentration and the angular velocity of the stage, ω (**Figure 2**a–c), as indicated on the phase diagram (Figure 2d). In part of the parameter space the droplet is able to transition to the magnet, while retaining a connection to the main ferrofluid reservoir via a liquid bridge. As the magnet continues to rotate the liquid bridge is stretched and a fiber is produced. However, when the viscosity of the fluid is too low the liquid bridge ruptures before a stable fiber is created (Figure 2b), while when the angular velocity of the stage is too large the droplet is unable to overcome the viscous and surface-tension forces and cannot attach to the magnet (Figure 2c). In both these cases, the process boundaries prohibit nanofiber fabrication.

We next explain the magnetospinning limits identified in Figure 2. The critical regime that enables a successful droplet transition from the syringe tip to the rotating stage will occur when the timescale of the rotating stage, $1/\omega$, exceeds the dynamic response timescale of the fluid droplet, R_d/v_r, where R_d is the droplet radius and v_r is the fluid response speed. For an external magnetic force F_m, we estimate $v_r = F_m/\eta R_d$ where η is the fluid viscosity. For a spherical magnet of volume V_m and magnetization M, $F_m \approx 3V_d\mu_0\chi V_m^2M^2/(\chi + 3)d^7$, where μ_0 is the permeability of free space, χ is the magnetic susceptibility of the suspension of nanoparticles, V_d is the volume of magnetic material contained within the droplet, and d is the closest separation between the fluid and the magnet.[12] Thus, the critical viscosity, η_c, that admits a successful droplet transition will satisfy the inverse relationship $\eta_c \leq A/\omega$, where $A = 4\pi\chi\phi R_d\mu_0V_m^2M^2/(\chi + 3)d^7$ and ϕ denotes the volume

Adv. Mater. 2015,
DOI: 10.1002/adma.201500374

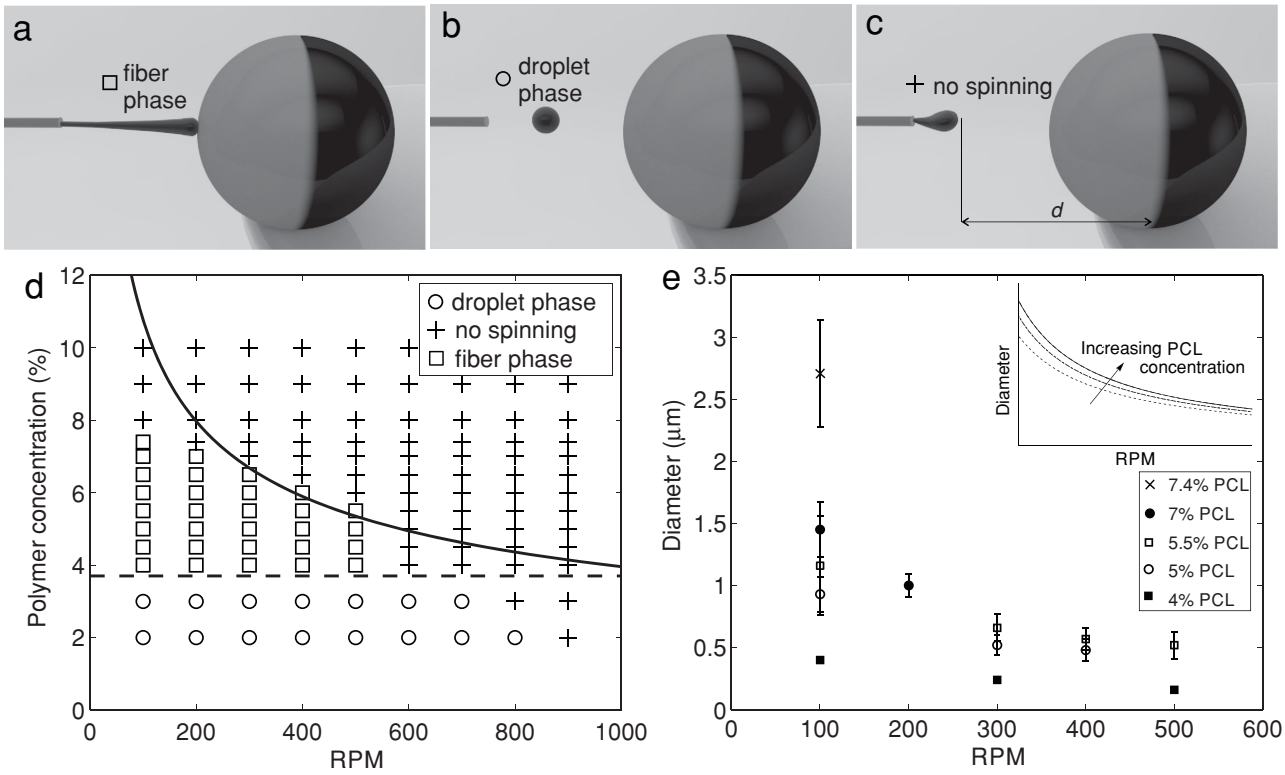

Figure 2. Three different regimes of the magnetospinning process. a) The droplet is attracted by the magnetic and a liquid bridge is stretched to form a stable nanofiber. b) The droplet transitions to the magnet without forming a liquid bridge. c) The magnet rotates too fast and the droplet is unable to attach to the magnet. d) The phase diagram of the PCL magnetospinning process with the theoretically predicted upper and lower bounds indicated by the solid and dashed curves, respectively, beyond which nanofiber spinning is prohibited. e) Mean diameters of the produced fibers versus angular velocity of the rotating stage. Error bars for 4% PCL fibers are smaller than the square marker. The inset demonstrates theoretical predictions based on Equation 1.

fraction of nanoparticles. The susceptibility and magnetization are each known only up to an order of magnitude, with $\chi \approx 10^{-3}$ and $M \approx 10^6$ A m^{-1}; fitting the resulting curve to the data predicts $\chi M^2/(\chi + 3) \approx 6 \times 10^9$ A^2 m^{-2}, which provides a quantitative parametric prediction for the upper bound in the phase plane where nanofiber spinning is prohibited, which agrees well with the experimental results (Figure 2d). We note that Tokarev et al.[13] provided a force diagram and a scaling law for the initial radius of the liquid bridge following a successful transition.

The location of the upper bound may be influenced by altering the concentration of nanoparticles within the fluid. An increase in the volume fraction of nanoparticles, ϕ, will increase the value of the parameter A in the relationship between viscosity and angular velocity. Assuming that variations in nanoparticle concentration do not affect the fluid viscosity, this implies that fibers with higher viscosities may be magnetospun by raising the concentration of magnetic nanoparticles (Figure S5, Supporting Information). In addition, the parametric dependence of A on the magnetic susceptibility of the nanoparticles indicates that similar effects may be achieved by using nanoparticles composed of different elements, such as cobalt or nickel, or by changing the size of the nanoparticles. We used 9 nm superparamagnetic nanoparticles to avoid aggregation problems in magnetic fields. However, larger ferromagnetic particles can be used in magnetospinning as well.

For the near-extensional flows characteristic of magnetospinning, we suggest that the lower bound in the phase diagram (dashed line in Figure 2d) is limited by a critical viscosity of solution below which capillary breakup of a thread occurs. This observation is consistent with an entanglement concentration, C_{cr}, since a stable jet of droplets is observed below that concentration.[14] Using available data, we estimated this critical entanglement concentration as C_{cr} = 3.7% (Figure S3, Supporting Information), which is in very good agreement with the experimental data.

Following the attachment of the fluid to the magnet, the continued rotation allows the liquid thread to be drawn out, which is accompanied by solvent evaporation and enables fabrication of magnetic fibers. Experiments were conducted for a range of stage rotation speeds to demonstrate the ability of magnetospinning to produce fibers with different diameters. The diameters of the fibers were estimated using scanning electron microscopy (SEM) images and ImageJ software, and the diameter was found to decrease both with increasing speed of rotation and with decreasing PCL concentration (Figure 2e). The finest nanofibers fabricated were 50 nm in diameter. The error bars in Figure 2e show the standard deviation for measurements of diameters of 50–70 different fibers produced in three independent experiments. In order to characterize the homogeneity of the fiber, we measured its diameter along the 25 cm length of the fiber for two fibers (Figure S6, Supporting

Information) and found that the homogeneity for both fibers was 2.5–5%.

During magnetospinning, nanofibers were collected on the reels glued along the edge of the rotating stage. The length of one nanofiber in the setup with stage radius R_s = 42 mm is $l = 2\pi R_s$ = 26 cm, so the magnetospinning setup produced a 26 cm long fiber with a single rotation. We also conducted a scale-up experiment with three needles located along the magnet rotation, which increased the production rate by a factor of 3–390 m min^{-1}.

The volume rate of production of fibers is given by $V_p = \pi R_f^2 [\pi R_s \omega k_1 k_2]$ where R_f is the fiber radius, k_1 is the number of feeding needles, and k_2 is the number of magnets on the stage. In Figure S4 (Supporting Information), we plot a series of curves for the production rate of the magnetospinning method depending on the diameter of the produced fibers and diameter of the rotating stage. As can be seen from Figure S4 (Supporting Information), the productivity rate per nozzle in magnetospinning is comparable with electrospinning (V_p = 0.04–0.2 cm^3 h^{-1}).[15] Scale-up of the system is possible by increasing the number of magnets and feeding needles at least to the density of one nozzle per centimeter, thus providing about 100 nozzles for an 80 mm radius rotating stage, and two orders of magnitude increased productivity.

The physics of magnetospinning can be modeled by accounting for surface tension, evaporation, and viscous effects in a stretching thread. As the stage rotates a force will be exerted perpendicular to the axis of the fiber, which will act to deform the fiber from its natural straight configuration. The relative effect of this compared with surface tension, which acts to straighten the fiber, is given by $\rho R^2 d\omega^2/\gamma \approx 10^{-5}$ for millimeter-radius fibers and so the fiber will remain straight during drawing.

We also assume that the fibers are slender, with radius $R(z)$, where $|dR/dz| \ll 1$, with speed $w(z)$, so that the process may be characterized by a classical extensional Trouton model, including evaporation:[16]

$$\frac{d}{dz}\left(R^2 w\right) = -\alpha R \tag{1a}$$

$$\frac{d}{dz}\left(3R^2 \eta \frac{dw}{dz}\right) + \gamma \frac{dR}{dz} = 0 \tag{1b}$$

Here, we assume that the evaporation rate is proportional to the exposed fiber surface, with a rate coefficient α. For the experiments conducted here, we measured $\alpha \approx 2 \times 10^{-6}$ ms^{-1}. Also, $z = 0$ is assigned to the position of the droplet at the pipette. In principle, there will also be an extra term in our stress balance that describes the viscoelastic polymeric contribution to the stress tensor (see, for example, ref. [17]). However, for the operating regimes of interest we expect to be in an approximately Newtonian regime (see Figure S2 and S3b, Supporting Information, which show, respectively, Newtonian behavior of the spinning solutions and a linear time dependence of the liquid thread diameter as a function of draw time).[18] Note that for Newtonian liquids, the extensional viscosity is three times the shear viscosity, as indicated by the Trouton ratio in Equation 1b. Three boundary conditions are required to solve the system (1). We prescribe the droplet radius at the needle tip, $R(0) = R_d$, and draw speed due to the stage rotation, $w(d) = R_s\omega$. Finally, to close the system, we assume that the velocity at which the fluid is drawn from the droplet to create the fiber is independent of rotation speed, so that $w(0)$ is a constant for all experiments, which may be determined by matching to the experimental data. This approach provides the final fiber radius for a given operating regime. A study of Equation 1 verifies that both the effect of surface tension and evaporation are necessary to explain the experimental observations in Figure 2e. In the absence of evaporation, Equation 1a predicts a decrease in fiber radius with the inverse square root of the draw speed. In the presence of evaporation, this effect is exacerbated further resulting in the potential for thinner fibers to be fabricated for equivalent draw speeds. The presence of surface tension in Equation 1b is essential to provide a dependence of the fiber radius on viscosity observed experimentally. When both of these effects are combined we are able to recreate the experimentally observed trends (Figure 2e, inset). In practice, additional measurements for a given experiment, such as the velocity at which fluid is drawn from the droplet and the particular behavior as the fiber solidifies and is wound onto the stage, could be used to give a quantitative comparison.

Even though many applications require highly loaded magnetic fibers,[19] it is advantageous to be able to produce fibers with lower loading of magnetic nanoparticles. The magnetic force withdrawing the droplet is dependent on the magnetic field gradient, and the concentration and magnetic properties of nanoparticles. By increasing the magnetic field gradient, we have found that the loading of magnetic particles can be decreased to 1 wt% magnetic nanoparticles dispersion. At this concentration no agglomerates of magnetic nanoparticles were observed at the surface of the fibers (Figure 1e). It has also been shown that such particle concentrations do not change the mechanical properties of the fiber, and in some cases can even improve them.[20]

Polymers with low dielectric constant cannot be electrospun without adding high dielectric constant ingredients but can be easily magnetospun, for example Teflon fluoropolymer fibers that are ideal for the design of superhydrophobic materials. The electrospinning methods can produce only core-shell Teflon fibers with a shell made of polyacrylonitrile, PVDF, and other polymer[21] because Teflon is soluble in liquids with very low dielectric constant (≈2). In contrast, here TAF 1600 (copolymer of 2,2-bis(trifluoromethyl)-4,5-difluoro-1,3-dioxole) in Fluorinert FC-40 fluid (dielectric constant = 1.9) was mixed with magnetic nanoparticles to magnetospin pure Teflon fibers with diameters ranging from 0.2 to 3 μm (**Figure 3**a). These magnetospun nanofibers demonstrate excellent superhydrophobic properties with contact angle = 157° (inset in Figure 3a).

In addition, we used a range of polymers, including polyethylene oxide, polystyrene, and poly(methyl methacrylate) (PMMA), to fabricate nanofibers (Figure 3b–d), including nanocomposite fibers filled with silver nanowires (Figure 3c) and multiwalled carbon nanotubes (MWCNT) (Figure 3d). The resulting fibers are naturally ferromagnetic, but the iron oxide nanoparticles may be etched to create a porous nonmagnetic fiber (Figure 3b). Alignment of carbon nanotubes in polymeric matrices has attracted great attention due to

Adv. Mater. 2015,
DOI: 10.1002/adma.201500374

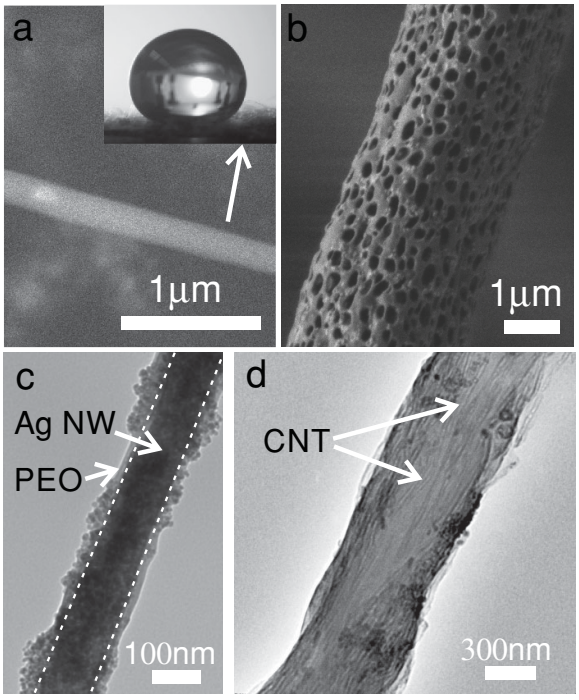

Figure 3. SEM and TEM images of fibers produced via magnetospinning. a) Magnetospun Teflon fiber. The inset shows water droplet on the mat for Teflon fibers. b) Porous non-magnetic PMMA fibers. c) PCL fiber with embedded silver nanowire (Ag NW) (1.7 wt% of silver nanowires). d) TEM image of poly(ethylene oxide) PEO fiber with embedded multi-walled carbon nanotubes (10 wt% of MWCNT).

dramatically increased tensile strength of the composite fibers.[22] We have shown that magnetospinning is capable of producing highly loaded continuous nanofibers with aligned nanowires and nanotubes (Figure 3c,d). The demonstrated examples show that our method enables new opportunities to design nanostructured materials at the level of single nanoparticulates of different shapes and dimensions.

In this work, we have presented a new method for spinning of continuous micro and nanofibers using a permanent revolving magnet. The method utilizes magnetic forces and hydrodynamic features of stretched threads to produce fine nanofibers. Scaling laws provide bounds for the operating regimes in which fibers may be fabricated, and theoretical models for the fiber drawing demonstrate the role of rotation speed, solution viscosity, evaporation, and surface tension in the fabrication process. In the range of 1–5% concentration in nanofibers, iron oxide nanoparticles have no effect on mechanical properties of the fibers.[20a] Iron oxide is biocompatible and biodegradable (see Figure S8, Supporting Information, which demonstrates fibroblast cells grown on the magnetospun scaffold with 5% iron oxide particles). The extra step of adding magnetic nanoparticles to the spinning solution is compensated by a number of advantages. The magnetospinning process is independent of the solution dielectric properties and requires no high voltages in contrast to the more traditional electrospinning technique. Magnetospinning is inexpensive, scalable, and simple, and the technique can be used for the fabrication of composite magnetic and non-magnetic porous fibers for a wide variety of applications. It is possible to build a magnetospinning setup, such as that used here, within minutes by simply combining an inexpensive rotating motor and a permanent magnet.

Experimental Section

Synthesis of Nanoparticles: Magnetic nanoparticles were synthesized by the co-precipitation method.[11c] In the synthesis process, 1.625 g (8 mmol) $FeCl_2{\cdot}4H_2O$ and 4.43 g (16 mmol) $FeCl_3{\cdot}6H_2O$ were dissolved in 190 mL water at room temperature while stirring. 10 mL of 25 wt% ammonia was added to the solution, which led to the formation of black magnetite precipitate. After 10 min of stirring, the precipitate was magnetically separated from solution and washed three times by deionized (DI) water.

Magnetic Nanoparticles Stabilized in Water: After the washing of magnetite nanoparticles (MNP) with HNO_3, the precipitate was diluted to 100 mL with water and the pH was raised to 2.5 with NaOH. 5 mL of a 0.5 M trisodium citrate dihydrate solution was added and the precipitate was stirred for 90 min, while maintaining the pH close to 2.5 with hydrochloric acid. The precipitate was separated by applying an external magnetic field and the supernatant was discarded. The precipitate was diluted to 50 mL with DI water and pH was raised to 6.

Magnetic Nanoparticles Stabilized in Chloroform: After washing in DI water, the MNP were additionally washed two times with ethanol and three times with chloroform. This was achieved by sequential precipitation of nanoparticles with a magnet and redispersion of the precipitate in solvent by sonication. Following the final cycle of precipitation, in which the supernatant was removed, a few droplets of oleic acid were added to wet the precipitate and the mixture was sonicated for 1 min with a high-power sonicator-homogenizer. The concentration of the MNP was 11.5% by weight and was measured by complete evaporation of chloroform in a vacuum oven at 100 °C.

Polymers in Chloroform: Stock solutions of polystyrene (PS) (M_w 280 000 g mol^{-1}, Sigma–Aldrich), PCL (M_n = 80 000 g mol^{-1}, Sigma–Aldrich), and PMMA (M_w = 300 000 g mol^{-1}, Sigma–Aldrich) in chloroform. The stock solutions were used to prepare formulations for spinning comprising 6 wt% polymer and 1.0–5.75 wt% nanoparticles. The mixtures were used for spinning after 1–2 h mixing.

Poly(ethylene oxide) (PEO) in Water/Ethanol: PEO (M_v = 400 000 g mol^{-1}) was dissolved in a mixture of water and ethanol (70/30) at 60 °C. Mixtures for fiber spinning were prepared by mixing 14 wt% PEO solution and citrate-stabilized MNP at a 1:1 ratio.

AgNW/PCL/MNP: Silver nanowires (Ag NW) with an average diameter of 90 nm and length of 20 μm provided by Blue Nano, USA were dispersed in chloroform at a concentration of 1.7%. Then, 30 wt% solution of PCL, 1.7 wt% AgNW dispersion, and 12 wt% dispersion of MNP were mixed in a 1:1:2 ratio. The spinning formulation contained 0.4 wt% AgNW, 5.75 wt% MNP, 7.5 wt% PCL in chloroform.

MWNT/PEO/MNP in Water: MWCNT were partially oxidized with a mixture of concentrated sulfuric and nitric acid (3:1 ratio) for 48 h at 80 °C. The MWCNT were rinsed four times with water and three times with ethanol, and dried in a vacuum oven at 110 °C. Following this, the MWCNT were redispersed to a concentration of 10% by weight in a citrate-stabilized magnetite nanoparticle dispersion using sonication. The obtained dispersion was stirred for 1 h with 14 wt% PEO solution. The spinning formulation contained 5 wt% MWNT, 4.5 wt% MNP, and 7 wt% PEO in water and ethanol (70:30).

High-Speed Imaging: Videos of the magnetospinning process were recorded on an Olympus i-SPEED FS camera at 10 000 fps and analyzed with VirtualDub software.

Supporting Information

Supporting Information is available from the Wiley Online Library or from the author.

Acknowledgements

This work was supported by funds of the University of Georgia. I.M.G. gratefully acknowledges support from Princeton University through a visiting lectureship position. The authors thank Celeste Nelson for a helpful conversation and Darya Asheghali for help with cell culture.

Received: January 23, 2015
Revised: March 31, 2015
Published online:

[1] a) M. M. Stevens, J. H. George, *Science* **2005**, *310*, 1135; b) L. Persano, C. Dagdeviren, Y. Su, Y. Zhang, S. Girardo, D. Pisignano, Y. Huang, J. A. Rogers, *Nat. Commun.* **2013**, *4*, 1633; c) D. Grafahrend, K.-H. Heffels, M. V. Beer, P. Gasteier, M. Möller, G. Boehm, P. D. Dalton, J. Groll, *Nat. Mater.* **2011**, *10*, 67.
[2] A. L. Yarin, B. Pourdeyhimi, S. Ramakrishna, *Fundamentals and Applications of Micro and Nanofibers*, Cambridge University Press, Cambridge, UK **2014**.
[3] L. Wadsworth, S. R. Malkan, *Int. Nonwovens Bull.: Tech. Textiles* **1991**, *2*, 46.
[4] R. K. Singh, K. D. Patel, J. H. Lee, E.-J. Lee, J.-H. Kim, T.-H. Kim, H.-W. Kim, *PLoS One* **2014**, *9*, e91584.
[5] A. L. Yarin, E. Zussman, *Polymer* **2004**, *45*, 2977.
[6] D. Yang, B. Lu, Y. Zhao, X. Jiang, *Adv. Mater.* **2007**, *19*, 3702.
[7] R. E. Rosensweig, *Ferrohydrodynamics*, Cambridge University Press, Cambridge, UK **1985**.
[8] a) K. Butter, P. H. H. Bomans, P. M. Frederik, G. J. Vroege, A. P. Philipse, *Nat. Mater.* **2003**, *2*, 88; b) A. J. Dickstein, S. Erramilli, R. E. Goldstein, D. P. Jackson, S. A. Langer, *Science* **1993**, *261*, 1012; c) J. V. I. Timonen, M. Latikka, L. Leibler, R. H. A. Ras, O. Ikkala, *Science* **2013**, *341*, 253; d) S. S. H. Tsai, I. M. Griffiths, Z. Li, P. Kim, H. A. Stone, *Soft Matter* **2013**, *9*, 8600.
[9] N. A. Clark, *Nature* **2013**, *504*, 229.
[10] a) C. Scherer, A. M. Figueiredo Neto, *Braz. J. Phys.* **2005**, *35*, 718; b) S. Safran, *Nat. Mater.* **2003**, *2*, 71; c) K. Raj, R. Moskowitz, *J. Magn. Magn. Mater.* **1990**, *85*, 233.
[11] a) A. Bumb, M. W. Brechbiel, P. L. Choyke, L. Fugger, A. Eggeman, D. Prabhakaran, J. Hutchinson, P. J. Dobson, *Nanotechnology* **2008**, *19*, 335601; b) O. Kudina, A. Zakharchenko, O. Trotsenko, A. Tokarev, L. Ionov, G. Stoychev, N. Puretskiy, S. W. Pryor, A. Voronov, S. Minko, *Angew. Chem. Int. Ed.* **2014**, *53*, 483; c) A. Tokarev, Y. Gu, A. Zakharchenko, O. Trotsenko, I. Luzinov, K. G. Kornev, S. Minko, *Adv. Funct. Mater.* **2014**, *24*, 4738.
[12] D. J. Griffiths, *Introduction to Electrodynamics*, Pearson, New York **2013**.
[13] A. Tokarev, W.-K. Lee, I. Sevonkaev, D. Goia, K. G. Kornev, *Soft Matter* **2014**, *10*, 1917.
[14] Q. P. Pham, U. Sharma, A. G. Mikos, *Tissue Eng.* **2006**, *12*, 1197.
[15] J. R. Venugopal, S. Low, A. T. Choon, A. B. Kumar, S. Ramakrishna, *Artif. Organs* **2008**, *32*, 388.
[16] a) F. T. Trouton, *Proc. R. Soc. London A* **1906**, *77*, 426; b) L. J. Cummings, P. D. Howell, *J. Fluid Mech.* **1999**, *389*, 361.
[17] J. Eggers, *Rev. Mod. Phys.* **1997**, *69*, 865.
[18] S. M. Berry, S. Pabba, J. Crest, S. D. Cambron, G. H. McKinley, R. W. Cohn, R. S. Keynton, *Polymer* **2011**, *52*, 1654.
[19] a) S. Liao, B. Li, Z. Ma, H. Wei, C. Chan, S. Ramakrishna, *Biomed. Mater.* **2006**, *1*, R45; b) D. Fragouli, A. Das, C. Innocenti, Y. Guttikonda, S. Rahman, L. Liu, V. Caramia, C. M. Megaridis, A. Athanassiou, *ACS Appl. Mater. Interfaces* **2014**, *6*, 4535; c) M. Bhaumik, H. J. Choi, R. I. McCrindle, A. Maity, *J. Colloid Interface Sci.* **2014**, *425*, 75; d) Y. Gu, K. G. Kornev, *Soft Matter* **2014**, *10*, 2816.
[20] a) M. Wang, H. Singh, T. A. Hatton, G. C. Rutledge, *Polymer* **2004**, *45*, 5505; b) M. Richard-Lacroix, C. Pellerin, *Macromolecules* **2013**, *46*, 9473.
[21] a) P. Muthiah, S.-H. Hsu, W. Sigmund, *Langmuir* **2010**, *26*, 12483; b) R. Scheffler, N. S. Bell, W. Sigmund, *J. Mater. Res.* **2010**, *25*, 1595.
[22] H. G. Chae, S. Kumar, *Science* **2008**, *319*, 908.